

Intrinsically Switched Varactor-Tuned Filters and Filter Banks

Andrew C. Guyette, *Member, IEEE*

Abstract—Intrinsically switched tunable filters are switched on and off using the tuning elements that tune their center frequencies and/or bandwidths, without requiring an increase in the tuning range of the tuning elements. Because external RF switches are not needed, substantial improvements in insertion loss, linearity, dc power consumption, control complexity, size, and weight are possible compared to conventional approaches. An intrinsically switched varactor-tuned bandstop filter and bandpass filter bank are demonstrated here for the first time. The intrinsically switched bandstop filter prototype has a second-order notch response with more than 50 dB of rejection continuously tunable from 665 to 1000 MHz (50%) with negligible passband ripple in the intrinsic off state. The intrinsically switched tunable bandpass filter bank prototype, comprised of three third-order bandpass filters, has a constant 50-MHz bandwidth response continuously tunable from 740 to 1644 MHz (122%) with less than 5 dB of passband insertion loss and more than 40 dB of isolation between bands.

Index Terms—Filters, microstrip filters, resonator filters, tunable circuits and devices.

I. INTRODUCTION

TUNABLE filters are essential to the realization of frequency-agile microwave systems. They are particularly useful in receiver applications because they can be reconfigured to adapt to a changing electromagnetic environment, capturing signals of interest while blocking unwanted interferers. There is a need for both high-performance tunable bandpass and bandstop filters, depending on the configuration and the specific requirements of the system [1].

When designing a tunable filter, there are several performance tradeoffs that must be considered. For example, as the tuning range of a tunable filter is widened, it becomes increasingly difficult to maintain a good filter response across the entire tuning range. This is due to two reasons: the frequency dependence of the filter's constituent parts (couplings, transmission-line electrical lengths, etc.) and the tuning-state dependence of the dissipative losses associated with the tuning elements, which tend to dominate over other losses in the filter. The frequency-dependence issue can be largely overcome with careful design [2]–[4], but the loss of the tuning elements sets fundamental performance limitations. As the tuning range of a tunable filter is increased, the tuning elements are necessarily

Manuscript received August 02, 2011; revised November 10, 2011; accepted November 18, 2011. Date of publication February 07, 2012; date of current version April 04, 2012.

The author is with Code 6851, Naval Research Laboratory, Washington, DC 20375-5347 USA.

Color versions of one or more of the figures in this paper are available online at <http://ieeexplore.ieee.org>.

Digital Object Identifier 10.1109/TMTT.2012.2184131

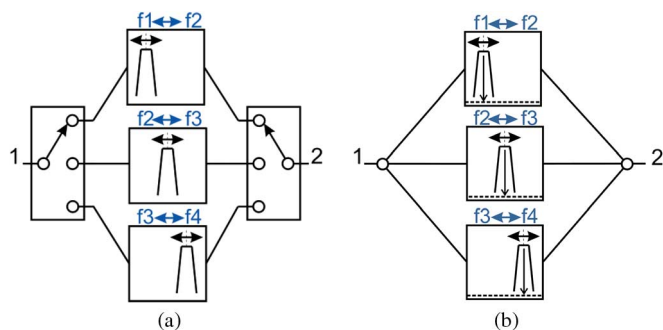


Fig. 1. (a) Conventional switched tunable bandpass filter bank. (b) Switchless tunable bandpass filter bank utilizing intrinsically switched tunable bandpass filters.

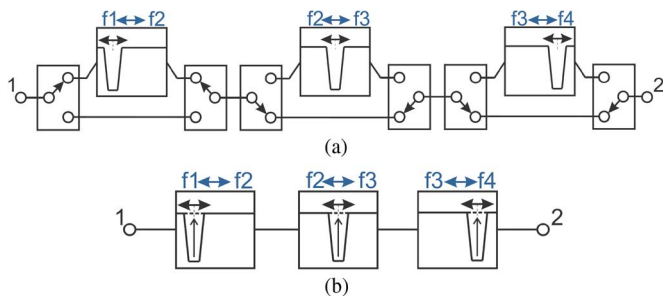


Fig. 2. (a) Conventional switched tunable bandstop filter bank. (b) Switchless tunable bandstop filter bank utilizing intrinsically switched tunable bandstop filters.

coupled more tightly to the resonators, and thus their loss has greater effect on the overall resonator unloaded Q (Q_u). A poor resonator Q_u results in a degradation of filter selectivity, as well as increased passband insertion loss in the case of bandpass filters and decreased stopband rejection in the case of bandstop filters. Passive loss compensation techniques do exist that allow for dramatic increases in the stopband rejection of lossy bandstop filters [5], but resonator Q_u still sets a lower limit to the 3-dB bandwidth.

In an attempt to extend the tuning range of tunable filters without degrading performance, switched-bank tunable filter configurations are often used. Switched tunable bandpass filter banks [see Fig. 1(a)] and switched tunable bandstop filter banks [see Fig. 2(a)] are comprised of a number of tunable filters with tuning ranges corresponding to bands within the desired full tuning range. To select the appropriate filter, RF switches are placed at the input and output in the bandpass bank, and before and after every filter in the bandstop bank. The result is superior performance, in terms of either total tuning range or passband insertion loss, to that which is possible with a single tunable

filter. The switches themselves, however, add significant passband insertion loss, which tends to increase as the number of filters in the bank increases, in the process significantly diminishing or eliminating the insertion loss improvement provided by reducing the tuning range of each of the individual constituent filters. In addition, the switches increase the size, weight, power consumption, and control complexity, and they can degrade the linearity of the filter bank. This paper proposes a solution to this problem in the form of intrinsically switched tunable filters, where the switching function is performed by the filters themselves, thereby completely eliminating the need for switches in filter banks [see Figs. 1(b) and 2(b)] and in other applications where a switchable filter is needed.

Intrinsically switched tunable filters are tunable filters that are switched on and off using the *same tuning elements* that tune their center frequencies and/or bandwidths. In its “off” state, an ideal intrinsically switched bandpass filter rejects signals of all frequencies, and an ideal intrinsically switched bandstop filter passes signals of all frequencies. A tunable bandpass filter with intrinsic-switching capability was first demonstrated in [6], where it is shown that varactors (tunable capacitors) can be used to tune not only the center frequency, but also the bandwidth, which could be tuned down to zero, effectively switching the filter off. This is achieved by using the varactors to control the voltage and current distributions in the resonators such that the electric and magnetic inter-resonator coupling coefficients are equal and opposite, resulting in zero net coupling. Microwave bandstop filters, however, are typically realized with a through-line with resonators coupled to it along its length. These resonator-to-through-line couplings cannot be cancelled in the same way as inter-resonator couplings in bandpass filters can be cancelled. This paper shows that intrinsically switched bandstop filters can, however, be realized with bandstop sections consisting of two transmission paths, where the bandstop response is suppressed with constructive interference.

This paper is organized into two main sections. Section II describes the theory of operation and design of intrinsically switched tunable bandstop filters, as well as the measured performance of a two-resonator microstrip prototype. The prototype gives a notch response with more than 50 dB of rejection continuously tunable from 665 to 1000 MHz (50%) with negligible passband ripple in the intrinsic off state. Section III describes in more detail the bandpass intrinsic switching concept first introduced in [6], and extends it to realize the first switchless tunable bandpass filter bank. A microstrip prototype comprised of three third-order intrinsically switched varactor-tuned bandpass filters was designed, built, and tested, and it demonstrated a constant 50-MHz 3-dB bandwidth response tunable from 740 to 1644 MHz (122%) with more than 40 dB of isolation, while requiring only five unique control signals. In both the bandstop Section II and the bandpass Section III, the coupling coefficient(s) versus varactor tuning characteristic of various tunable filter topologies is evaluated. Such analyses are greatly simplified with the assumption that the couplings are relatively weak, which results in simple expressions representative of the tuning characteristics of the different circuit topologies. Once a tunable filter topology with the desired tuning charac-

teristics is identified, the design process can proceed with more representative equivalent circuits and/or computer simulation.

II. INTRINSICALLY SWITCHED TUNABLE BANDSTOP FILTERS

Switched bandstop filters are conventionally realized using switches to bypass a bandstop filter with a through-line, as in Fig. 2(a). This approach requires that the switches are in the signal path, where the switches add significant passband insertion loss in both the on and off states. An alternative approach is presented in [7], where switches are used instead to switch in a bandpass filter in parallel with a bandstop filter, which results in an all-pass response. As the bandstop filter is never switched out of the circuit, the switches are not required to be in the signal path in the on state. However, the approach in [7] has two limitations. First, the all-pass condition necessary for the off state determines the bandstop transfer function, and thus, bandstop responses with optimum selectivity for a given application (e.g., elliptic function) cannot necessarily be realized. Second, in the off state, this approach gives a *resonant* all-pass response, which means that significant group-delay ripple is present around the center frequency of the suppressed bandstop response. Group-delay variation can cause signal distortion, as well as increased insertion loss from the dissipative losses of the circuit elements. The intrinsically switched tunable filters, described here, do not suffer from these limitations. In addition, they are both center frequency and bandwidth tunable, neither of which is true for the filters shown in [7].

In [8], the higher order spurious responses of bandstop filters are cancelled using the constructive interference associated with a two-path bandstop section. In this paper, it is shown that this technique can also be applied to cancel out the fundamental bandstop response in a controlled fashion and thus allow for the realization of intrinsically switched bandstop filters. The properties of two-path bandstop sections are discussed in Section II-A. Sections II-B and II-C describe the theory and design of an intrinsically switched bandstop section, and a microstrip prototype is presented in Section II-D.

A. Two-Path Bandstop Section

A high-pass prototype of a conventional bandstop section is shown in Fig. 3(a). It consists of a 1-F capacitor, which represents a resonator, coupled to a transmission line of $1-\Omega$ characteristic impedance with an admittance inverter K_0 . Using conventional circuit analysis [9] and assuming a $1-\Omega$ source and load impedance, the transfer function is found to be

$$S_{21} = e^{-j(\theta_1 + \theta_2)} \frac{p}{p + \frac{K_0^2}{2}} \quad (1)$$

where $p = \alpha + j\omega$ is the complex frequency variable and θ_1 and θ_2 are the electrical lengths of the input and output through-line sections. The 3-dB cutoff frequency of the high-pass prototype is

$$\omega_c = \frac{K_0^2}{2} \quad (2)$$

and thus the bandwidth of a conventional bandstop section is dependent only on the strength of the coupling K_0 .

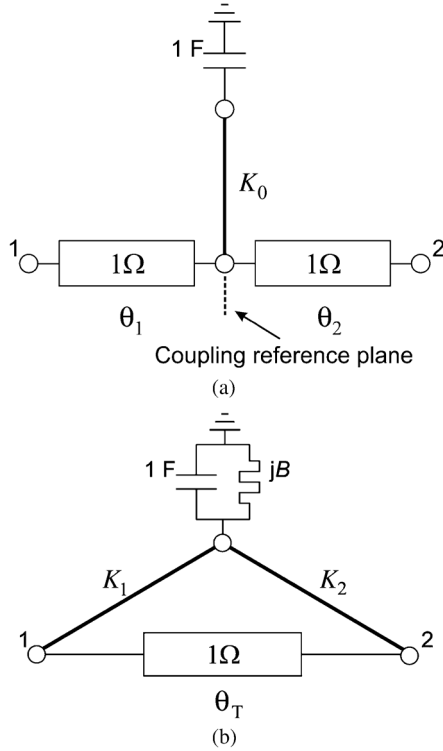


Fig. 3. (a) Conventional bandstop section—bandwidth is dependent on the strength of coupling K_0 only. (b) Two-path bandstop section—bandwidth is dependent on K_1 , K_2 , and θ_T .

A high-pass prototype of a two-path bandstop section is shown in Fig. 3(b), comprised of a resonator coupled twice, with couplings K_1 and K_2 , to a through-line of $1\text{-}\Omega$ characteristic impedance and electrical length θ_T . The frequency shift of the resonator is modeled by a shunt frequency-invariant susceptance B . Under the condition

$$B = K_1 K_2 \sin \theta_T \quad (3)$$

the frequency of zero transmission in the high-pass prototype transfer function is normalized to the origin. The transfer function is then

$$S_{21} = e^{-j\theta_T} \frac{p}{p + \frac{1}{2}(K_1^2 + K_2^2 + 2K_1 K_2 \cos \theta_T)} \quad (4)$$

and the reflection functions are

$$S_{11} = -\frac{\frac{1}{2}e^{-2j\theta_T}(e^{j\theta_T}K_1 + K_2)^2}{p + \frac{1}{2}(K_1^2 + K_2^2 + 2K_1 K_2 \cos \theta_T)} \quad (5)$$

$$S_{22} = -\frac{\frac{1}{2}e^{-2j\theta_T}(e^{j\theta_T}K_2 + K_1)^2}{p + \frac{1}{2}(K_1^2 + K_2^2 + 2K_1 K_2 \cos \theta_T)}. \quad (6)$$

The 3-dB cutoff frequency is

$$\omega_c = \frac{1}{2}(K_1^2 + K_2^2 + 2K_1 K_2 \cos \theta_T) \quad (7)$$

which is dependent on both the values of the couplings K_1 and K_2 , as well as θ_T , the electrical length of the through-line. The

bandstop response of this section is turned off ($\omega_c = 0$, $|S_{21}| = 1$) when

$$\theta_T = \cos^{-1} \frac{-(K_1^2 + K_2^2)}{2K_1 K_2}. \quad (8)$$

In the off state, the resonator is effectively removed from the circuit, leaving only the through-line. This is also true when the resonator has finite Q_u , which can be modeled by the change of variable $p \rightarrow p + G$ in (4), where G is a shunt conductance representing resonator loss.

The conventional and two-path bandstop sections are equivalent when

$$K_0 = \sqrt{K_1^2 + K_2^2 + 2K_1 K_2 \cos \theta_T} \quad (9)$$

and

$$\theta_1 = \frac{1}{2} \left(\pi - \arg \left(-\frac{K_1}{K_2} + e^{-j\theta_T} \right) \right) \quad (10)$$

$$\theta_2 = \theta_T - \theta_1. \quad (11)$$

Therefore, the reference plane for the coupling of the equivalent conventional bandstop section, defined by θ_1 and θ_2 , is dependent on the relative strength of the couplings K_1 and K_2 .

The two-path bandstop section possesses two properties of interest: it becomes a through-line when constructive interference occurs between the two paths (when (8) is satisfied), and the coupling reference plane [from (10) and (11)] may be controlled by controlling the ratio of the couplings K_1 and K_2 . Both of these properties are used to realize intrinsically switched bandstop filters, as described in Sections II-B and II-C.

B. Effect of Mixed Coupling on the Coupling Reference Plane

Here it is shown that a resonator coupled to a through-line with a mix of both electric and magnetic couplings can be modeled as the two-path bandstop section of Fig. 3(b), where K_1 and K_2 represent the electric and magnetic couplings, respectively. Consequently, the coupling reference plane is determined by the relative strength of the electric and magnetic couplings.

Fig. 4(a) depicts a resonator coupled to a normalized transmission line with both electric coupling (represented by mutual capacitance C_m) and magnetic coupling (represented by mutual inductance L_m). An equivalent circuit is shown in Fig. 4(b), where the electric and magnetic couplings are represented by an admittance inverter k_C and an impedance inverter k_L , respectively. This is a simplification since both couplings are assumed here to be to the same point on the transmission line, where, in a realizable microwave circuit, the couplings would be distributed along the length of a transmission line, and the negative elements of the inverters would be absorbed by modifying the transmission line's equivalent capacitance and inductance per unit length. However, this simplified circuit is useful for understanding the effects of changing the ratio of electric to magnetic coupling. For example, at resonance, when there is only electric coupling ($k_L = 0$), the circuit of Fig. 4(b) reduces to a shunt-series lumped-element resonator, and thus at resonance there is an RF short at the point at which the resonator couples to the through-line. Conversely, when there is only magnetic coupling

($k_C = 0$), the circuit reduces to a series-parallel lumped-element resonator, which becomes an RF open at resonance. Transitioning between pure electric coupling (a short) to pure magnetic coupling (an open) is equivalent to a 90° phase shift along the through-line. This observation is used to derive the equivalent two-path bandstop section high-pass prototype shown in Fig. 4(c), where the admittance inverters K_a and K_b are given by

$$K_a = \frac{k_C}{\sqrt{b}} = \frac{k_C}{\sqrt{\omega_0 C_1}} \quad (12)$$

$$K_b = \frac{k_L}{\sqrt{x}} = \frac{k_L}{\sqrt{\omega_0 L_1}} \quad (13)$$

where b and x are the susceptance and reactance slope parameters [11] of the resonator, respectively. K_a and K_b were derived by assuming $k_L = 0$ and $k_C = 0$, respectively, and therefore the high-pass prototype is only valid for weak couplings. Referring to Fig. 3 and setting $\theta_T = 90^\circ$, $K_1 = K_a$, and $K_2 = K_b$, the frequency shift [from (3)] and K_0 [from (9)] of the equivalent conventional bandstop section [see Fig. 3(a)] are given by

$$B = k_C k_L \quad (14)$$

and

$$K_0 = \sqrt{K_a^2 + K_b^2} = \sqrt{\frac{k_C^2}{\omega_0 C_1} + \frac{k_L^2}{\omega_0 L_1}}. \quad (15)$$

Equation (15) shows that for the conventional bandstop section topology, the electric and magnetic couplings are additive regardless of their relative sign and ω_c [from (2)] cannot be zero, given any nonzero amount of either electric or magnetic coupling, no matter what the ratio of electric to magnetic coupling is. The coupling reference plane is defined by θ_1 and θ_2 , given by (10) and (11). The value of θ_1 ranges from 0° (when $k_L = 0$) to 90° (when $k_C = 0$).

C. Realization of an Intrinsically Switched Tunable Bandstop Section

As just demonstrated, the coupling reference plane of a resonator coupled to a through-line is related to the ratio of electric to magnetic coupling. If this ratio were to be made tunable, the coupling reference plane would also be tunable. Furthermore, if such a resonator is coupled to a through-line twice, with two mixed couplings (as in Fig. 4) with tunable electric to magnetic ratios, a two-path bandstop section [as in Fig. 3(b)] could be realized where the through-line electrical length θ_T is tunable, and thus, intrinsically switchable if θ_T can be tuned to satisfy (8).

A convenient and practical way of tuning the ratio of electric to magnetic coupling is with the use of a transmission-line resonator loaded with two varactors and side coupled to a through-line. Offset tuning the varactors—in other words, varying the ratio of their respective capacitances—changes the distribution of voltage and current in the distributed coupling region, which, in turn, changes the ratio of electric to magnetic coupling.

1) *Analysis of a Side-Coupled Offset-Tuned Transmission-Line Resonator:* Shown in Fig. 5(a) is the well-known equivalent circuit of a pair of coupled lines [10], comprised of shorted stubs of characteristic admittance y_{12} and unit elements of ad-

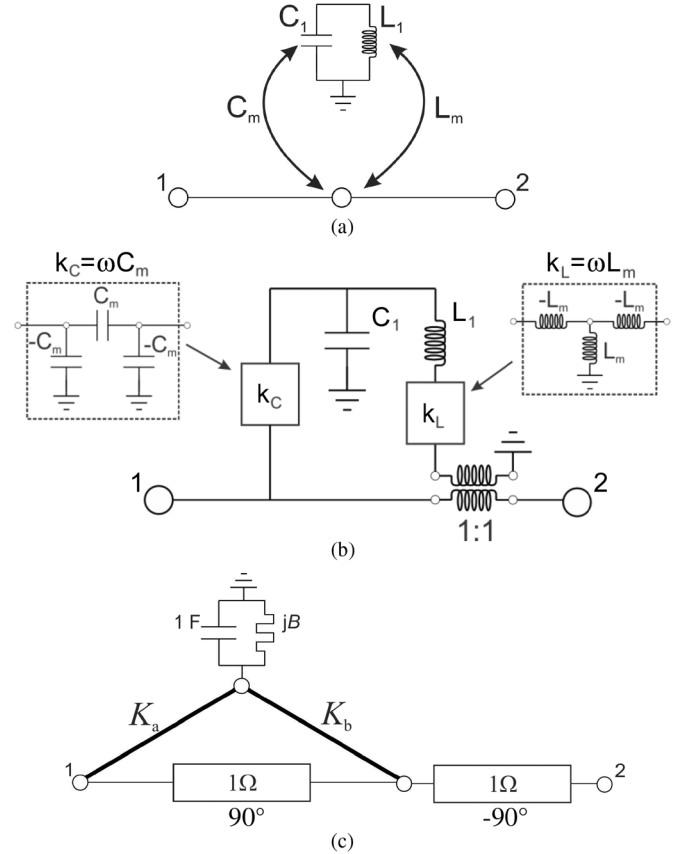


Fig. 4. (a) General representation of a resonator coupled to a through-line with both electric and magnetic couplings. (b) Equivalent circuit comprised of an admittance inverter k_C and an impedance inverter k_L . (c) High-pass prototype, comprised of a two-path bandstop section and a 90° phase shift.

mittances $-y_{12}$, y_{11} , and y_{22} . The two unit elements of admittance $-y_{12}$ can be replaced with the equivalent network of Fig. 5(b) [9, p. 171] consisting of an admittance inverter and two shorted stubs. A resulting new coupled-line model consisting of two unit elements and four admittance inverters is shown in Fig. 5(c).

Fig. 6(a) is a schematic representation of a side-coupled capacitively loaded transmission-line resonator coupled from one end to a through-line over an electrical length θ_{AB} . The coupling region is modeled using the admittance inverter equivalent circuit of Fig. 5(c). The electrical length of the resonator at its fundamental resonant frequency, ω_0 , is θ_0 . A varactor with capacitance C_1 is attached to one end of the resonator, and a varactor with capacitance C_2 to the opposite end. The characteristic admittance of the resonator along its entire length is defined to be y_{11} , and the characteristic impedance of the through-line is normalized to 1Ω . Assuming weak coupling, the voltage and current distributions on the transmission-line resonator at resonance can be defined to be continuous sinusoidal standing waves with amplitudes

$$V = \cos \theta \quad (16)$$

$$I = y_{11} \sin \theta \quad (17)$$

where θ is the electrical length referred to the left end of the resonator in Fig. 6(a). θ_{C1} and θ_{C2} are electrical lengths of open

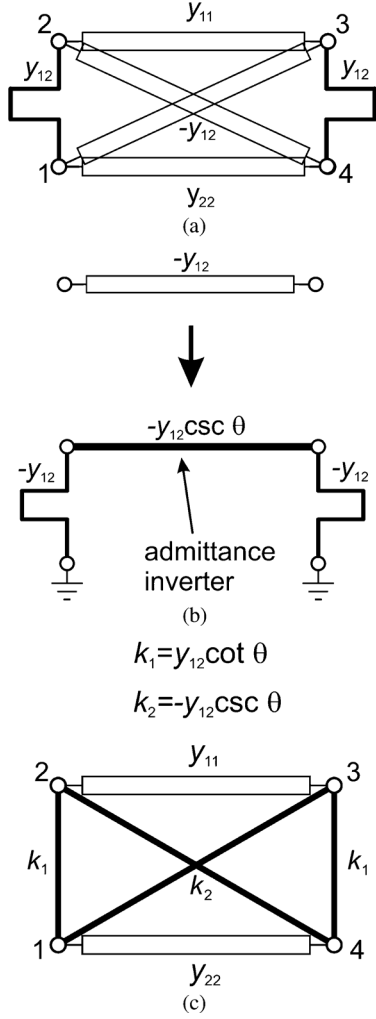


Fig. 5. Derivation of admittance inverter model of coupled-line section. (a) Model derived from admittance matrix [7]. (b) Transformation of unit element. (c) Admittance inverter model.

stubs equivalent to C_1 and C_2 , respectively, at the resonant frequency, ω_0

$$\theta_{C1} = \tan^{-1} \frac{\omega_0 C_1}{y_{11}} \quad \theta_{C2} = \tan^{-1} \frac{\omega_0 C_2}{y_{11}} \quad (18)$$

and

$$\theta_{C1} + \theta_{C2} = \pi - \theta_0. \quad (19)$$

Therefore, for a given θ_0 , increasing θ_{C1} decreases θ_{C2} and vice versa. From (18), C_1 and C_2 are given by

$$C_1 = \frac{y_{11} \tan \theta_{C1}}{\omega_0} \quad (20)$$

$$C_2 = \frac{y_{11} \tan \theta_{C2}}{\omega_0}. \quad (21)$$

Next, the susceptance slope parameters b_A and b_B , looking into the resonator at nodes A and B, the points at which the admittance inverters connect to the resonator, are calculated. The standard expression for the susceptance slope parameter b is [11, p. 430]

$$b = \left(\frac{\omega_0}{2} \right) \frac{dB}{d\omega} \Big|_{\omega \rightarrow \omega_0} \quad (22)$$

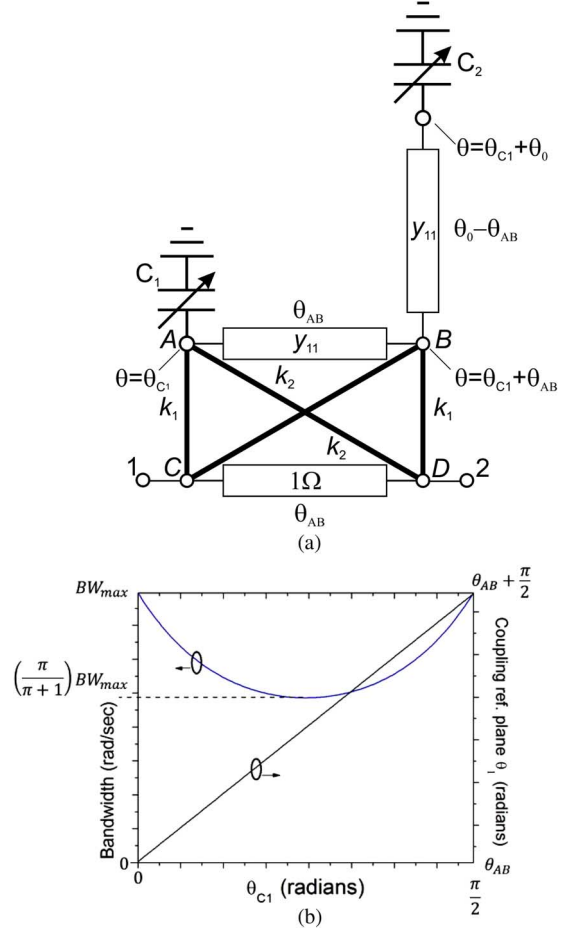


Fig. 6. (a) Schematic representation of an offset-tuned transmission-line resonator side coupled to a through-line using coupled-line equivalent circuit of Fig. 5. (b) Calculated bandwidth and coupling reference plane response with offset tuning ($\theta_0 = \pi/2$, $\theta_{AB} = \theta_0/2$).

where ω is angular frequency, ω_0 is the resonant frequency, and B is the resonator susceptance. The derivative of susceptance with respect to frequency may be written in terms of stored energy [12, p. 232]

$$\frac{dB}{d\omega} \Big|_{\omega \rightarrow \omega_0} = \frac{4(W_m + W_e)}{V^2} \quad (23)$$

where W_m and W_e are the stored magnetic and electric energies, respectively, in the resonator at resonance, and V is the voltage amplitude at the input node at resonance. Equation (22) can then be written

$$b = \left(\frac{\omega_0}{2} \right) \frac{dB}{d\omega} \Big|_{\omega \rightarrow \omega_0} = \left(\frac{\omega_0}{2} \right) \frac{4(W_m + W_e)}{V^2}. \quad (24)$$

Recognizing that at resonance the stored electric and magnetic energies are equal

$$W_e = W_m \quad (25)$$

gives

$$b = \frac{4\omega_0 W_m}{V^2} \quad (26)$$

and thus using (16),

$$b_A = \frac{4\omega_0 W_m}{\cos^2 \theta_{C1}} \quad (27)$$

$$b_B = \frac{4\omega_0 W_m}{\cos^2(\theta_{AB} + \theta_{C1})}. \quad (28)$$

The stored magnetic energy W_m is calculated by integrating the energy stored in the inductance per unit length (L') over the length of the resonator in a similar fashion to that done in [6], [13], and [14]

$$\begin{aligned} W_m &= \frac{L'}{4} \int_{l_{C1}}^{l_0+l_{C1}} I^2 dl \\ &= \frac{L' y_{11}^2}{4} \int_{l_{C1}}^{l_0+l_{C1}} \sin^2 \beta l dl \\ &= \frac{y_{11}}{16\omega_0} (2\theta_0 + \sin 2\theta_{C1} - \sin 2(\theta_0 + \theta_{C1})) \end{aligned} \quad (29)$$

where the current I is given by (17), β is the phase constant, and

$$L' y_{11}^2 = C' = y_{11} \frac{\beta}{\omega_0} \quad (30)$$

$$l_0 = \frac{\theta_0}{\beta} \quad l_{C1} = \frac{\theta_{C1}}{\beta}. \quad (31)$$

The resonator, at nodes A and B, is coupled to the through-line with admittance inverters k_1 and k_2 , effectively forming the two-path bandstop section of Fig. 3(b) with normalized couplings

$$K_1 = \frac{k_1}{\sqrt{b_A}} + \frac{k_2}{\sqrt{b_B}} \text{sgn}(V_A V_B) \quad (32)$$

$$K_2 = \frac{k_2}{\sqrt{b_A}} + \frac{k_1}{\sqrt{b_B}} \text{sgn}(V_A V_B). \quad (33)$$

The $\text{sgn}(V_A V_B)$ terms are included to take into account the effect of phase shift across the resonator, where V_A and V_B are given by (16) evaluated at nodes A and B, respectively. Recognizing that only the relative sign of K_1 and K_2 needs to be preserved and using (27) and (28) and referring to Fig. 5(c), (32) and (33) can be simplified to

$$K_1 = \frac{y_{12} \sin \theta_{C1}}{\sqrt{4\omega_0 W_m}} \quad (34)$$

$$K_2 = -\frac{y_{12} \sin(\theta_{AB} + \theta_{C1})}{\sqrt{4\omega_0 W_m}}. \quad (35)$$

The cutoff frequency of the equivalent high-pass prototype is given by (7) with $\theta_T = \theta_{AB}$

$$\omega_c = \frac{y_{12}^2 \sin^2 \theta_{AB}}{8\omega_0 W_m}. \quad (36)$$

The coupling reference plane is defined by (10)

$$\theta_1 = \frac{1}{2} \left(\pi - \arg \left(-\frac{K_1}{K_2} + e^{-j\theta_{AB}} \right) \right) = \theta_{AB} + \theta_{C1} \quad (37)$$

which shows that, for a given tuned center frequency, the coupling reference plane is determined by the relative values of C_1 and C_2 , and that offset-tuning can shift the reference plane by up to 90° (since $0 < \theta_{C1} < \pi/2$). Offset tuning C_1 and C_2 has only a moderate effect on the bandwidth, and bandwidth cannot be tuned down to zero when either C_1 or C_2 is nonzero [see Fig. 6(b)].

2) *Analysis of an Intrinsically Switched Bandstop Section:* It has just been demonstrated that the offset tuning of two varactors attached to a side-coupled bandstop resonator shifts the coupling reference plane. This property can be used to indirectly control the through-line electrical length θ_T of the two-path bandstop section of Fig. 3(b) by shifting the reference planes of the couplings K_1 and K_2 . This can be achieved by side coupling a transmission-line resonator loaded with two varactors twice to a through-line, in a manner such that offset tuning the varactors shifts the two coupling reference planes in opposite directions, such as done in the circuit shown in Fig. 7(a). As the varactors C_1 and C_2 are offset tuned, the coupling reference planes for the two side couplings shift in opposite directions along the through-line with respect to one another, effectively changing the through-line length between them, thereby realizing the two-path bandstop filter section of Fig. 3(b) with a tunable θ_T .

Shown in Fig. 7(b) is the circuit of Fig. 7(a) simplified by first reducing it to two two-path bandstop high-pass prototype sections sharing a single resonator using (34) and (35), and then, using (9), calculating K_0 for each two-path section

$$K_0 = \frac{y_{12} \sin \theta_{AB}}{\sqrt{4\omega_0 W_m}} \quad (38)$$

with frequency offset calculated from (3)

$$B = \frac{y_{12}^2}{4\omega_0 W_m} \sin^2 \theta_{AB} \sin(2\theta_{AB} + 2\theta_{C1} + \theta_3). \quad (39)$$

The 3-dB cutoff frequency of the equivalent high-pass prototype is then

$$\omega_c = \frac{y_{12}^2 \cos^2(\theta_{AB} + \frac{\theta_3}{2} + \theta_{C1}) \sin^2 \theta_{AB}}{2\omega_0 W_m} \quad (40)$$

which can be tuned down to zero by changing the value of θ_{C1} (offset tuning). Shown in Fig. 7(c) is a plot of C_1 and C_2 versus tuned center frequency (represented by resonator electrical length θ_0) calculated from solving (40) for θ_{C1} for both constant absolute bandwidth and intrinsic off states. For the constant absolute bandwidth state, C_1 and C_2 are equal at the lowest tuned center frequency, but not at the highest. Ideally C_1 and C_2 should converge at both the upper and lower tuned center frequencies (assuming C_1 and C_2 represent the capacitances of identical devices), and thus the full tuning range of both devices is utilized. However, if a constant absolute bandwidth is not needed, it may be possible, depending on passband bandwidth requirements, to utilize the full tuning ranges of identical varactors using this circuit topology. Another solution would be to use two different devices, or differently coupled identical devices, with different tuning ranges. Note that there are values of

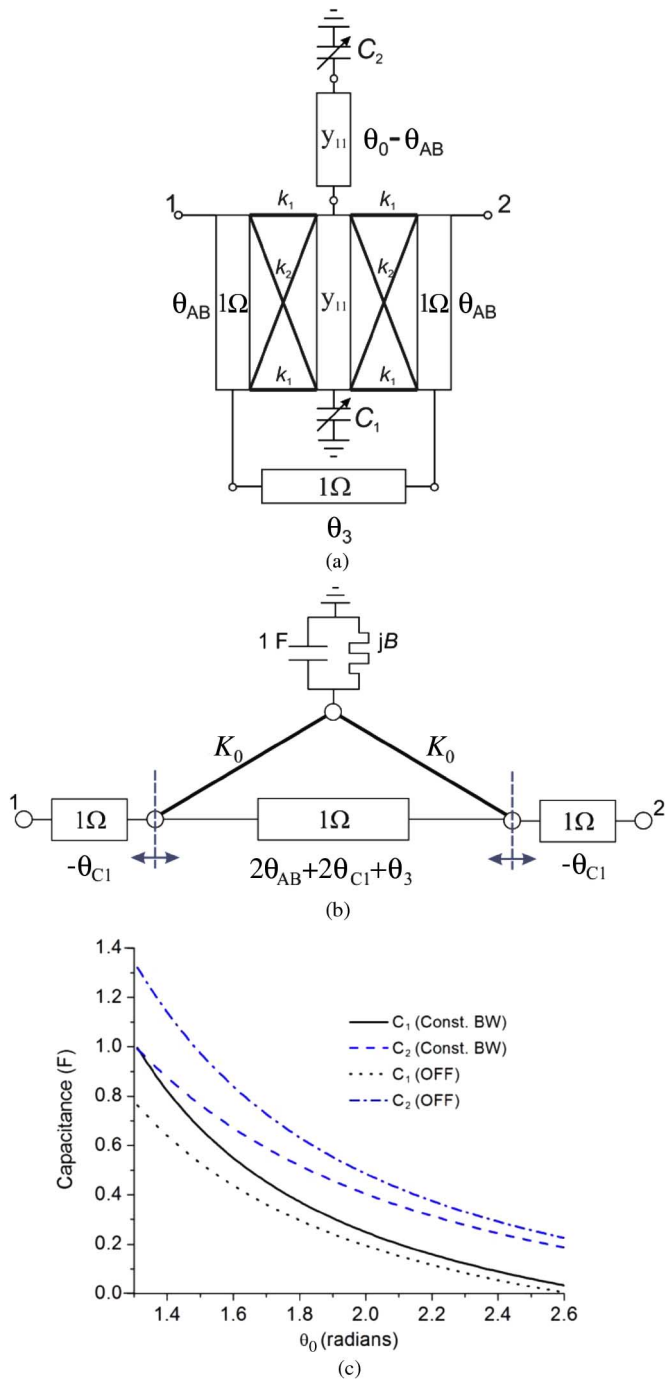


Fig. 7. Intrinsic switched bandstop section. (a) Schematic representation. (b) Equivalent circuit high-pass prototype—a two-path bandstop section [see Fig. 3(b)] with θ_T dependent on offset tuning. (c) Calculated tuning curves for varactors C_1 and C_2 versus center frequency, for constant absolute bandwidth and intrinsic off states with $\theta_{AB} = 0.6\theta_0$ and the y_{11}/ω_0 term in (20) and (21) normalized to 1.

C_1 and C_2 for the intrinsic off state that lie within the values of the constant absolute bandwidth state—which demonstrates that an increase in the tuning range of the varactors is not required for intrinsic switching using this topology.

D. Second-Order Intrinsic Switched Tunable Notch Prototype

A second-order intrinsic switched notch filter prototype based on the intrinsic switched bandstop section shown in

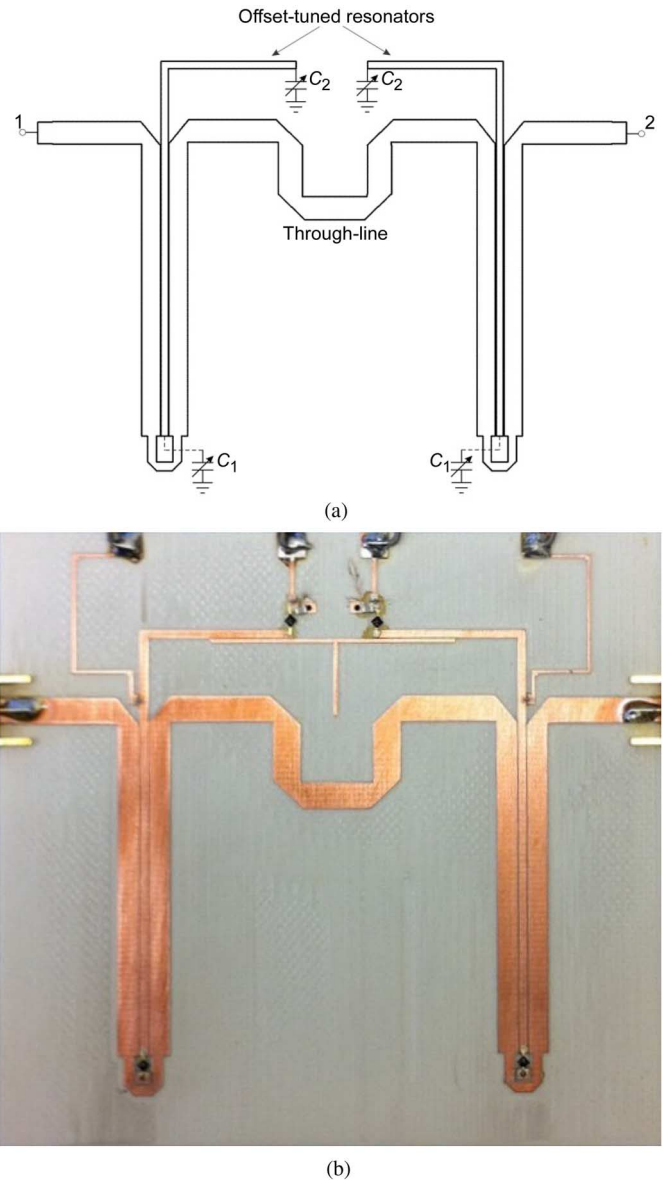


Fig. 8. Intrinsic switched tunable notch prototype. (a) Simplified layout. (b) Fabricated circuit of overall dimension 8.6 cm \times 8.1 cm.

Fig. 7(a) was designed, built, and tested. A simplified layout of the prototype is shown in Fig. 8(a) (bias lines are not shown). It consists of two intrinsic switched bandstop sections in cascade, with a small amount of coupling introduced between the two resonators, which has the effect of significantly increasing the notch depth by adding a small amount of destructive interference [5]. Design and simulation was done using AWR Microwave Office and SONNET. The width and length of the resonators is 1.1 and 78 mm, respectively. The coupled-line spacing for all couplings is 0.1 mm and the length of the coupled-line sections is 45.1 mm. The width of the through-line in the coupled-line sections is 2.8 mm. The through-line connecting the two bandstop sections is 53.3-mm long and 3.2-mm wide. It was found from simulation that in order to obtain good return loss across the entire passband, it was necessary to decrease the width of the short length of through-line at the bottom of the bandstop sections (adjacent to C_1) to 1.3 mm. Shown

in Fig. 8(b) is the fabricated circuit. The substrate is Rogers Duroid 4003 (thickness = 1.52 mm, $\epsilon_r = 3.38$). The varactors are Aeroflex/Metelics MGV-125-24-E25 ($C_j = 0.35 - 7.3$ pF, $V_{br} = 20$ V, $Q_{50 \text{ MHz}} = 3000$). Coilcraft 0302CS 34-nH surface mount inductors, ATC 600S 100-pF chip capacitors, and Vishay 100-k Ω chip resistors are used in the low-pass bias networks.

Shown in Fig. 9 are the simulated and measured results. The bandwidth is tunable from 143 MHz down to 25.5 MHz, while maintaining at least 50 dB of rejection [see Fig. 9(a)], the center frequency is tunable from 665 to 1000 MHz [see Fig. 9(b)], and the return loss is better than 25 dB in the intrinsic off state [see Fig. 9(c)]. In this intrinsic-off state measurement, the resonators are tuned to 725 MHz, but the bandstop response is completely suppressed. Shown in Fig. 10 are two-tone third-order intermodulation product measurements for both an on state (a center frequency of 800 MHz and a bandwidth of 35 MHz) and an intrinsic off state where the resonators are tuned to 800 MHz. This measurement was taken with one tone centered in the middle of the stopband at 800 MHz and the other tone swept. The power of both tones was set to 0 dBm at the input. The measured linearity of the on state is relatively poor, which is to be expected when semiconductor varactors are used as tuning elements. The measured intermodulation product level in the intrinsic off state is the noise floor of the measurement. All S -parameter and linearity measurements were taken with an Agilent N5247A PNA-X network analyzer.

It should be noted that although the total through-line length of this prototype is longer than that of a comparable conventional second-order bandstop filter, the through-line length of higher order intrinsically switched bandstop filters can be minimized with the use of the hybrid reflection-mode filter topology [9, p.303].

III. INTRINSICALLY SWITCHED TUNABLE BANDPASS FILTER BANK

An intrinsically switched tunable bandpass filter uses tuning elements to not only tune the center frequency and/or bandwidth, but also to control the relative values of the inter-resonator electric and magnetic coupling coefficients, which when equal and opposite result in zero net coupling and the filter is switched off. This section presents a simplified analysis of two intrinsically switched tunable resonator topologies first presented in [6], as well as the design and measured results of the first switchless tunable bandpass filter bank.

In [15], switches are used at the output of a bandpass filter to switch in a delay line, which turns the filter off with signal cancellation. Drawbacks of this approach include the fact that the filter is not tunable, and the switching function requires adding additional components. In [16] and [17], switched filters and filter banks are presented in which switches are attached to resonators inside each filter instead of being used to select filters at the input and output of the bank. These switches are used to severely detune the resonant frequencies of the resonators, and in doing so turn the filters off. The couplings, however, are not cancelled, which limits the maximum isolation that can be

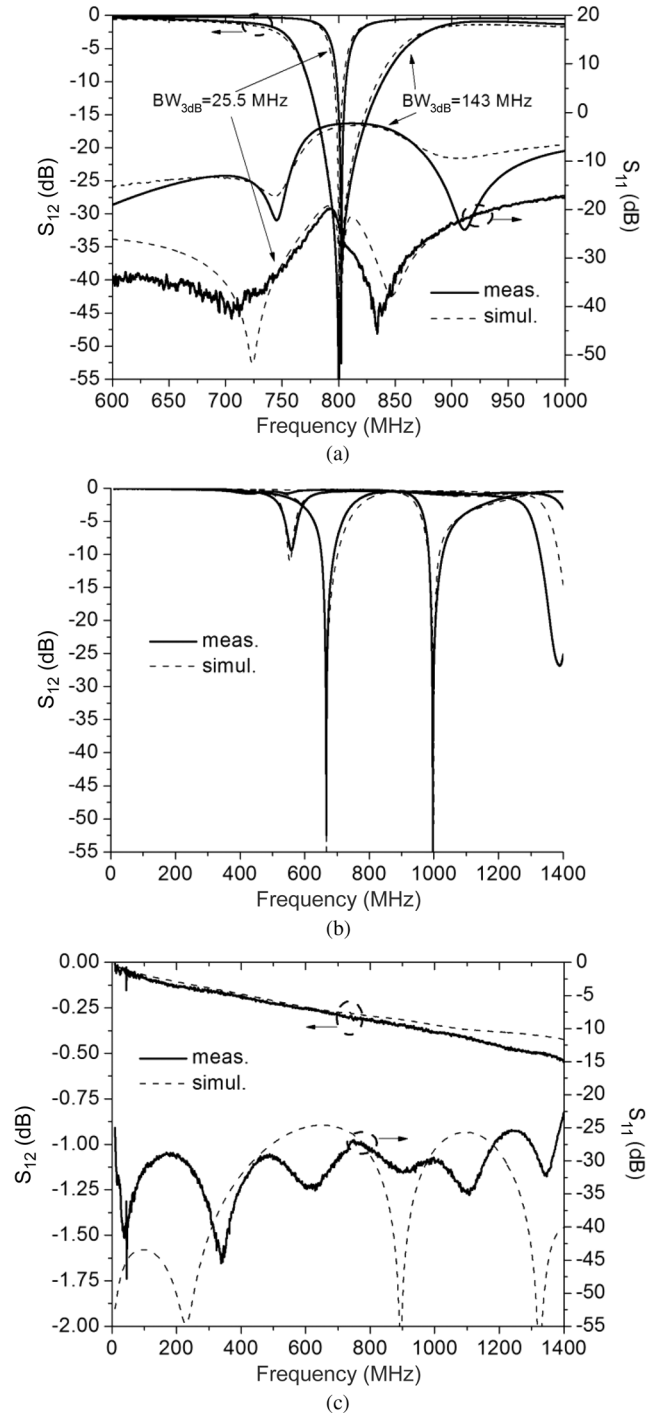


Fig. 9. Intrinsically switched tunable notch filter prototype simulated and measured results. (a) Bandwidth tuning. (b) Center frequency tuning. (c) Intrinsic off state.

achieved, as the detuned resonators basically function as non-resonating nodes. The approach described in this paper is distinct in that the resonators are not required to be detuned at all, but instead the couplings are cancelled. In the case of tunable filters and filter banks, this is a significant advantage in that the filters can be switched on and off with all the resonators tuned within the center frequency tuning range of a filter, and thus the switching function is achieved without an insertion loss penalty,

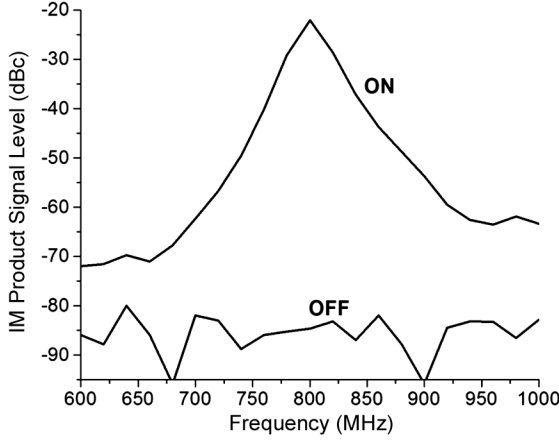


Fig. 10. Third-order intermodulation product two-tone measurements of the intrinsically switched tunable notch for both the on state (center frequency is 800 MHz, 3-dB bandwidth set to 35 MHz) and the intrinsic off state. Power of the input tones is 0 dBm, and one tone is fixed in the center of the stopband (800 MHz) and the other tone is swept.

as an increase in the tuning range of the tuning elements is not required.

A. Intrinsically Switched Resonator Topologies

This section presents a simplified analysis, similar to that done of the intrinsically switched bandstop filters (Section II-C), of the intrinsically switched resonator topologies first presented in [6]. From this analysis, varactor tuning curves for the constant absolute bandwidth and intrinsic off states are derived.

1) *Analysis of Varactor-Tuned Parallel-Coupled Transmission-Line Resonators:* The standard definition of the coupling coefficient between two resonators is [11, p. 433]

$$K = \frac{k_{12}}{\sqrt{b_1 b_2}} \quad (41)$$

where k_{12} is the admittance of the inverter representing the coupling, and b_1 and b_2 are the susceptance slope parameters of the two resonators. Shown in Fig. 11(a) is a pair of varactor-loaded transmission-line resonators, each identical in form to the offset-tuned transmission-line resonator considered in Section II-C, coupled to each other over an electrical length θ_{AB} from one end. The coupling region is modeled using the coupled-line admittance inverter model of Fig. 5(c). Assuming weak coupling, the voltages and currents in the resonators at resonance are unaffected by the presence of the admittance inverters k_1 and k_2 , and thus the total coupling coefficient can be written

$$K = \frac{k_1}{b_A} + \frac{k_1}{b_B} + 2 \frac{k_2}{\sqrt{b_A b_B}} \text{sgn}(V_A V_B) \quad (42)$$

where b_A and b_B are the susceptance slope parameters looking into the resonator at nodes A and B , respectively, and are given by (27) and (28). As in Section II-C, the $\text{sgn}(V_A V_B)$ term is included to take into account the effect of phase shift across the resonator. Equation (42) simplifies to

$$K = \frac{y_{12} \cos(\theta_{AB} + 2\theta_{C1}) \sin \theta_{AB}}{4\omega_0 W_m} \quad (43)$$

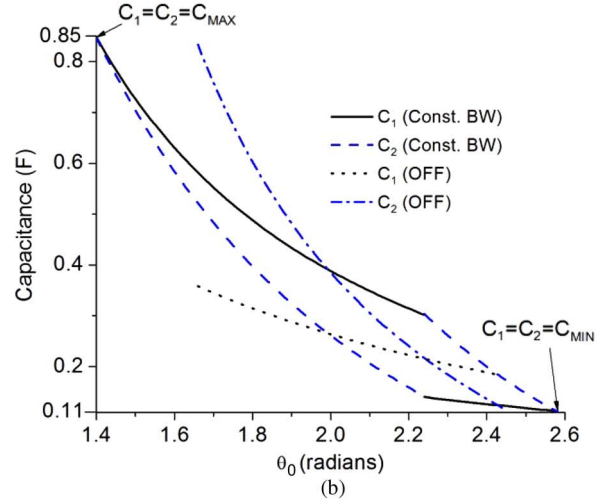
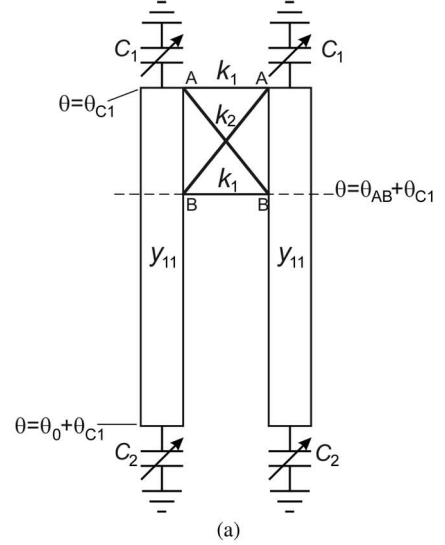


Fig. 11. Symmetric pseudocombine intrinsically switchable resonator topology. (a) Schematic. (b) Calculated normalized varactor tuning curves for constant absolute bandwidth and intrinsic off states with $\theta_{AB} = 0.3\theta_0$ and the y_{11}/ω_0 term in (20) and (21) normalized to 1.

The coupling coefficient K is zero (the intrinsic off state) when

$$\theta_{C1} = \frac{\pi}{4} - \frac{\theta_{AB}}{2} \quad (44)$$

The coupling bandwidth is

$$\text{BW} = \omega_0 K. \quad (45)$$

Shown in Fig. 11(b) are varactor tuning curves for a constant absolute bandwidth state and the intrinsic off state, derived using (43) and (45) where C_1 and C_2 are given by (20) and (21). Note that C_1 and C_2 exchange values near the high end of the tuning range. The pseudocombine topology exhibits an “optimum” tuning curve, where C_1 and C_2 are equal at both the minimum and maximum tuned center frequencies, and thus the full range of all tuning elements is used for center frequency tuning.

Shown in Fig. 12(a) is another intrinsically switchable coupled-resonator topology, comprised of an offset-tuned pseudocombine resonator and a nonoffset-tuned combline resonator.

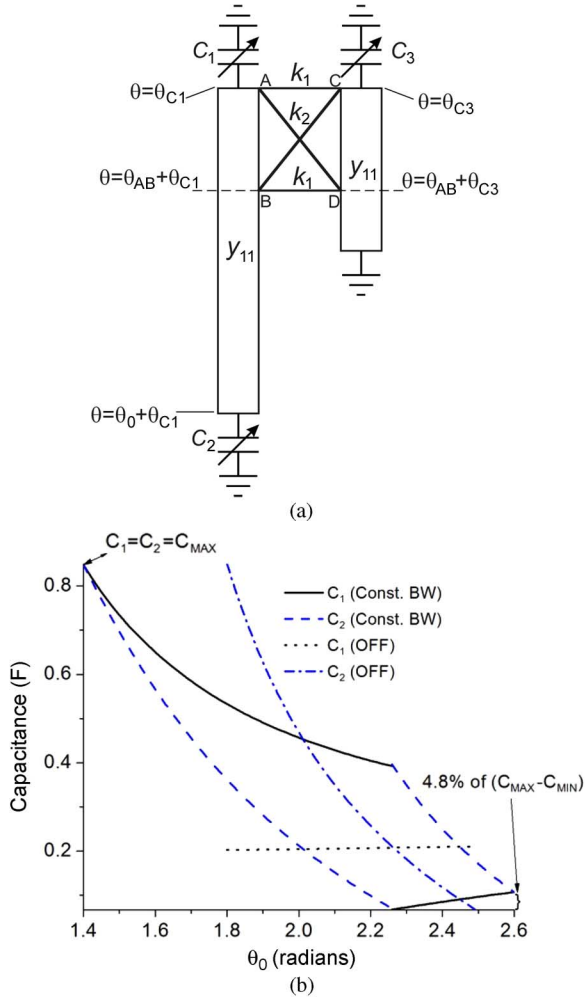


Fig. 12. Mixed pseudocombine/combine intrinsically switchable resonator topology. (a) Schematic. (b) Calculated normalized varactor tuning curves for constant absolute bandwidth and intrinsic off states with $\theta_{AB} = 0.3\theta_0$ and the y_{11}/ω_0 term in (20) and (21) normalized to 1.

The magnetic energy stored in the nonoffset-tuned combline resonator is

$$W_{mc} = \frac{L'}{4} \int_0^{\frac{l_0}{2}} \cos^2 \beta l \, dl = \frac{y_{11}}{16\omega_0} (\theta_0 + \sin \theta_0) \quad (46)$$

which is calculated using (30) and (31). The coupling coefficient is then

$$\begin{aligned} K &= k_1 \left(\frac{\text{sgn}(V_A V_C)}{\sqrt{b_A b_C}} + \frac{\text{sgn}(V_B V_D)}{\sqrt{b_B b_D}} \right) \\ &\quad + k_2 \left(\frac{\text{sgn}(V_A V_D)}{\sqrt{b_A b_D}} + \frac{\text{sgn}(V_B V_C)}{\sqrt{b_B b_C}} \right) \\ &= \frac{y_{12} \cos(\theta_{AB} + \theta_{C1} + \theta_{C3}) \sin \theta_{AB}}{8\omega_0 \sqrt{W_{mc} W_m}} \end{aligned} \quad (47)$$

where

$$\theta_{C3} = \frac{\pi - \theta_0}{2}. \quad (48)$$

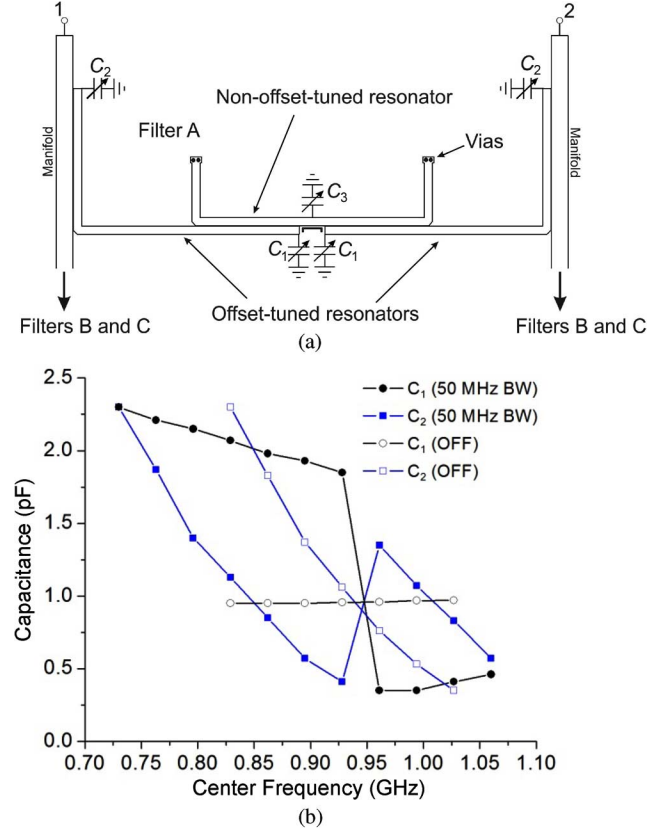


Fig. 13. (a) Simplified layout of Filter A (low-band). (b) Simulated varactor tuning curves for the on and intrinsic off states.

The coupling coefficient of the mixed coupled-resonator topology is dependent on the cosine of θ_{C1} , while the coupling coefficient of the symmetric pseudocombine topology is dependent on the cosine of $2\theta_{C1}$, and thus the latter is more sensitive to offset tuning, which is to be expected as both resonators are offset tuned in the symmetric pseudocombine topology. The tuning curves for a constant-absolute bandwidth of the mixed topology, shown in Fig. 12(b), are somewhat less than optimum, sacrificing 4.8% of the total varactor tuning range. Although nonideal in this regard, this topology allows for a very practical realization, as shown in Section III-B. Also, note that C_1 for the intrinsic off state is nearly constant for the full tuning range of C_2 , which simplifies varactor bias control.

B. Intrinsically Switched Tunable Filter Bank Prototype

An intrinsically switched tunable bandpass filter bank microstrip prototype was designed, built, and tested to demonstrate the feasibility of an intrinsically switched filter bank. The prototype is comprised of three third-order intrinsically switched bandpass filters (Filters A–C) coupled to shorted-circuit-terminated transmission-line manifolds at the input and output. Shown in Fig. 13(a) is a simplified layout of the low-band filter (Filter A), tunable from 750 to 1075 MHz. This filter is based on the mixed pseudocombine/combine topology of Fig. 12(a) with the two outer resonators being offset-tuned pseudocombine, and the central resonator being essentially two nonoffset-tuned combline resonators connected in parallel. The width and length of all the resonators is 1.6

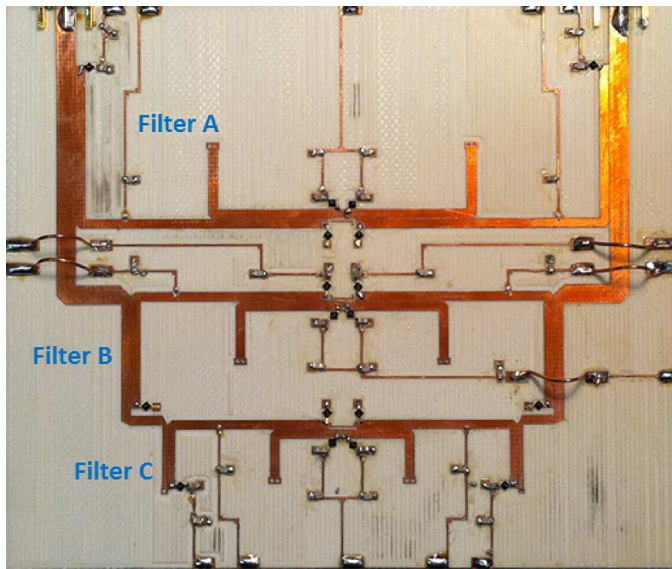


Fig. 14. Fabricated intrinsically switched tunable bandpass filter bank prototype of overall dimension 11.9 cm \times 10.1 cm.

and 71.1 mm, respectively. The coupled-line spacing for all couplings is 0.1 mm, and the length of the inter-resonator and input/output couplings is 20.7 and 28.3 mm, respectively. It was observed in simulation that the cross-coupling between the two offset-tuned resonators was primarily inductive (due to the loading of the varactors) and thus a small length of a capacitively coupled high-impedance transmission line was added in between them to increase the capacitive coupling, and thus increase the isolation. AWR Microwave Office was used for the preliminary design; the final design was done in SONNET. The lengths of the input and output side-couplings were optimized in AWR to provide decent passband return loss across the entire tuning range. In this prototype, the input and output couplings are not cancelled in the intrinsic off state, although this should be possible using the techniques of Section II and is an area for future research. Shown in Fig. 13(b) is the simulated varactor-capacitance tuning curves of Filter A for the 50-MHz bandwidth on state and intrinsic off state [note the correspondence with Fig. 12(b)]. The capacitance range of Fig. 13(b) corresponds to a tuning voltage range of approximately 3–20 V. The geometries of filters B and C are simply scaled-down versions of Filter A with minor modifications to the input/output coupling lengths to take into account impedance changes along the manifolds. The varactor tuning voltage range of Filter B is 4–20 V and the varactor tuning voltage range of Filter C is 5–20 V.

Shown in Fig. 14 is the fabricated circuit. The substrate is Rogers Duroid 4003 (thickness = 1.52 mm, $\epsilon_r = 3.38$). The varactors are Aeroflex/Metelics MGV-125-24-E25 ($C_j = 0.35 - 7.3$ pF, $V_{br} = 20$ V, $Q_{50\text{ MHz}} = 3000$). Coilcraft 0302CS 34-nF surface mount inductors and ATC 600S 100-pF chip capacitors are used in the bias networks. Although there are a total of 15 bias lines in this circuit, only five unique control voltages are needed for standard operation (only one filter on at a time)—one for each C_1 varactor pair, one for all the C_2 varactors, and one for all the C_3 varactors.

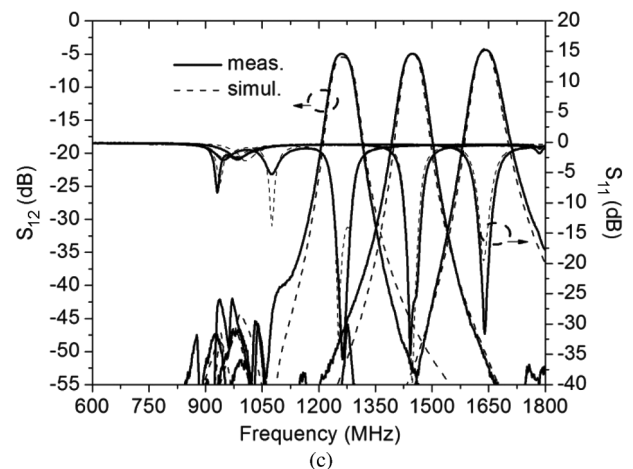
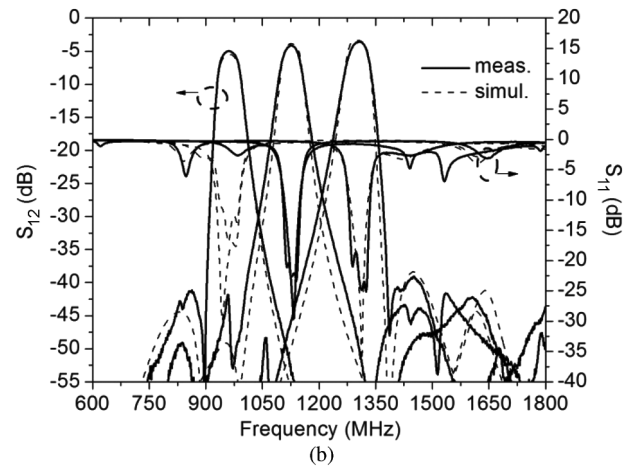
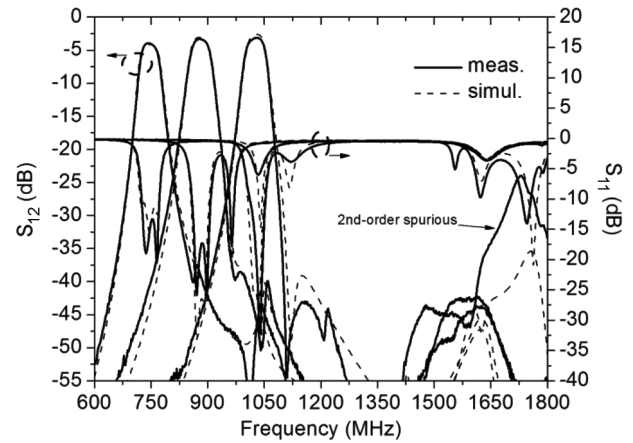


Fig. 15. Intrinsically switched tunable bandpass filter bank prototype simulated and measured results. (a) Filter A on. (b) Filter B on. (c) Filter C on.

Shown in Fig. 15 are simulated and measured results of the bank showing the tuning ranges of the individual filters, with the other two filters intrinsically switched off. The passband bandwidth is a constant 50 MHz, with more than 40 dB of isolation between filters. The 25-dB spurious response in the upper stopband of Filter A is due to second-order spurious of the filter itself, not from interaction with the other filters. Shown in Fig. 16(a) and (b) are measurements showing the full composite tuning range, and shown in Fig. 16(c) are simulated and measured results with all three filters on simultaneously

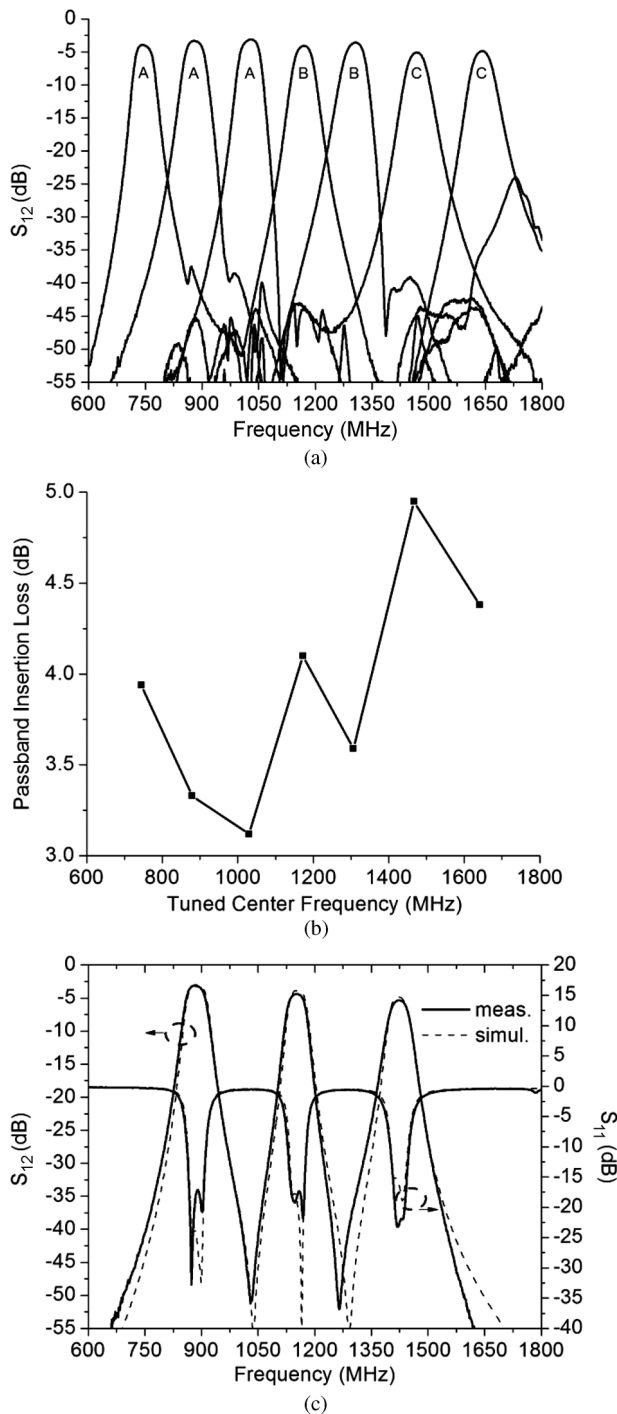


Fig. 16. Intrinsicly switched tunable bandpass filter bank prototype results. (a) Measured full tuning range. (b) Measured passband insertion loss versus tuned center frequency. (c) All filters on simultaneously.

(which required a unique control voltage for each of the C_3 varactors, for a total of seven control voltages). Shown in Fig. 17 are two-tone intermodulation measurements for Filter B tuned to 1000 MHz, in both the on state (50-MHz 3-dB bandwidth) and the intrinsic off state. The linearity, which is typical of varactor-diode-tuned filters, could be improved with the use of circuit techniques, such as using back-to-back varactor diodes with specific doping profiles [18]. There is still measurable intermodulation in the intrinsic-off state, as only

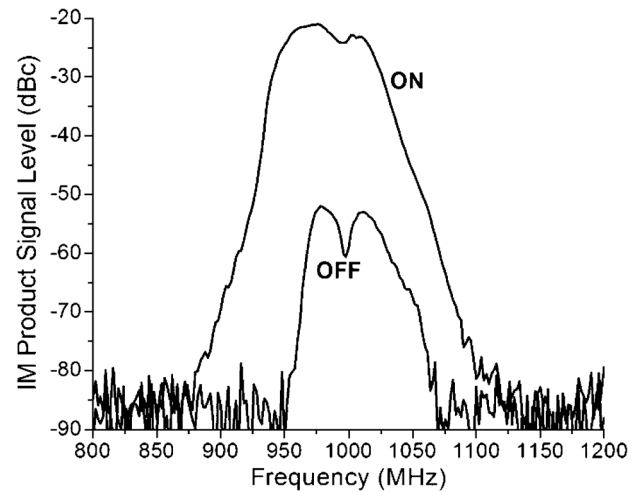


Fig. 17. Third-order intermodulation product two-tone measurements of Filter B of the intrinsicly switched tunable bandpass filter bank prototype for both the on state (center frequency is 1000 MHz, 3-dB bandwidth set to 50 MHz) and the intrinsic off state. Power of the input tones is 0 dBm, and they are spaced 1 MHz apart and both swept simultaneously.

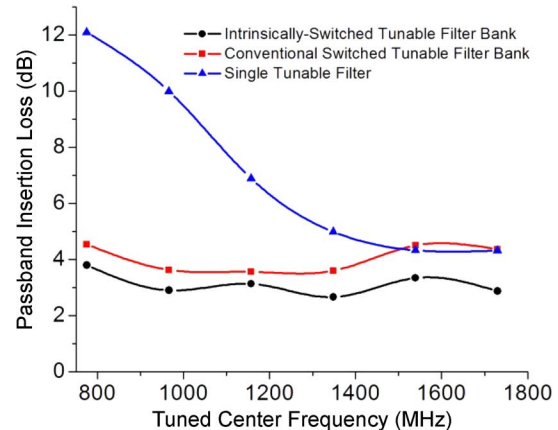


Fig. 18. Simulated passband insertion loss versus tuned center frequency of the intrinsicly switched tunable bank compared to conventional approaches.

the inter-resonator couplings are cancelled in this prototype, and thus significant signal power still reaches the varactors of the input resonator of the filter. An Agilent N5247A PNA-X network analyzer was used for the S -parameter and linearity measurements.

Shown in Fig. 18 is a plot of simulated passband insertion loss versus tuned center frequency for the intrinsicly switched tunable filter bank, a conventional switched filter bank, and a single tunable filter, all using the same microstrip substrate and varactors and covering the same frequency range. The single tunable filter is a conventional combline filter design, as are the three filters in the conventional switched tunable bank. The switch used in the simulation of the conventional switched bank is the NEC uPG2150T5L (GaAs MMIC SP3T, 0.1–8.1 GHz). The maximum instantaneous passband bandwidths are set to 50 MHz. From this comparison, the advantage of using a filter bank over a single tunable filter is obvious, as is the advantage of using the intrinsicly switched bank over the conventional switched bank, with an insertion loss improvement that ranges from 0.5 to 1.5 dB. While moderate, it should be kept in

mind that the absolute insertion loss difference between these particular conventional and switchless banks would remain unchanged if the filters were realized using lower loss technology (e.g., suspended stripline resonators and higher Q varactors) as the extra loss of the conventional bank is primarily due to the losses of the switches. If the number of filters in the conventional and switchless banks is increased, the absolute insertion loss difference between them would also increase due to the increased loss of the higher throw or cascaded switches in the conventional bank. The intrinsically switched bank approach removes the switch-loss-imposed upper limit to the number of filters that can be used, and thus realizing low-loss tunable filter banks comprised of large numbers of low-loss narrow-tuning-range filters becomes a problem of manifold design rather than the much more difficult problem of realizing low-loss high-throw or cascaded switches.

IV. CONCLUSION

This paper has demonstrated an intrinsically switched tunable bandstop filter and an intrinsically switched tunable bandpass filter bank for the first time. Intrinsically switched tunable bandstop filters are shown to be realizable with a two-path bandstop section. An intrinsically switched bandstop filter prototype is presented that gives a second-order notch response with more than 50 dB of rejection continuously tunable from 665 to 1000 MHz (50%) with negligible passband ripple in the intrinsic off state. An intrinsically switched tunable bandpass filter bank prototype is presented, which is comprised of three third-order filters, and gives a constant 50-MHz bandwidth response continuously tunable from 740 to 1644 MHz (122%) with less than 5 dB of passband insertion loss and more than 40 dB of isolation. The insertion-loss performance of the intrinsically switched tunable filter bank could be improved with the addition of more intrinsically switched filters. It is expected that intrinsically switched tunable filters and filter banks will play an important role in the realization of future high-performance microwave systems.

ACKNOWLEDGMENT

The author would like to thank D. Jachowski, Naval Research Laboratory, Washington, DC, for the interesting technical discussions and encouragement, as well as for his invaluable assistance in editing this paper's manuscript.

REFERENCES

- [1] P. Wong and I. Hunter, "Electronically tunable filters," *IEEE Microw. Mag.*, vol. 10, no. 1, pp. 46–54, Jan. 2009.
- [2] I. C. Hunter and J. D. Rhodes, "Electronically tunable microwave bandpass filters," *IEEE Trans. Microw. Theory Tech.*, vol. MTT-30, no. 9, pp. 1354–1360, Sep. 1982.
- [3] S.-J. Park and G. M. Rebeiz, "Low-loss two-pole tunable filter with three different predefined bandwidth characteristics," *IEEE Trans. Microw. Theory Tech.*, vol. 56, no. 5, pp. 1137–1148, May 2008.
- [4] D. R. Jachowski and A. C. Guyette, "Sub-octave-tunable microstrip notch filter," in *Proc. IEEE Int. Electromagn. Compat. Symp.*, 2009, pp. 99–102.
- [5] D. R. Jachowski, "Compact, frequency agile, absorptive bandstop filters," in *IEEE MTT-S Int. Microw. Symp. Dig.*, Jun. 2005, pp. 513–516.
- [6] A. C. Guyette, "Alternative architectures for narrowband varactor-tuned bandpass filters," in *Eur. Microw. Conf.*, Oct. 2009, pp. 1828–1831.
- [7] J. D. Rhodes, "Switched bandstop filters," *Int. J. Circuit Theory Appl.*, vol. 22, pp. 107–120, 1994.
- [8] A. C. Guyette, "Design of fixed- and varactor-tuned bandstop filters with spurious suppression," in *Eur. Microw. Conf.*, Oct. 2010, pp. 288–291.
- [9] I. C. Hunter, *Theory and Design of Microwave Filters*. London, U.K.: IEE Press, 2001.
- [10] R. Sato and E. G. Cristal, "Simplified analysis of coupled transmission-line networks," *IEEE Trans. Microw. Theory Tech.*, vol. MTT-18, no. 3, pp. 122–131, Mar 1970.
- [11] G. Matthaei, L. Young, and E. M. T. Jones, *Microwave Filters, Impedance-Matching Networks, and Coupling Structures*. Norwood, MA: Artech House, 1980.
- [12] R. E. Collin, *Foundations for Microwave Engineering*. New York: McGraw-Hill, 1992.
- [13] V. V. Tyurnev, "The coupling coefficients of an asymmetric pair of microwave resonators," *J. Commun. Technol. Electron.*, vol. 35, no. 1, pp. 1–8, 2002.
- [14] M. A. Sanchez-Soriano, E. Bronchalo, and G. Torregrosa-Penalva, "Parallel-coupled line filter design from an energetic coupling approach," *IET Microw. Antennas Propag.*, vol. 5, no. 5, pp. 568–575, Apr. 2011.
- [15] W.-H. Tu, "Switchable microstrip bandpass filters with reconfigurable frequency responses," in *IEEE MTT-S Int. Microw. Symp. Dig.*, Jun. 2010, pp. 1488–1491.
- [16] P. D. Laforge, R. R. Mansour, and M. Yu, "Manifold-coupled switched filter bank implementing filters with embedded switches," in *IEEE MTT-S Int. Microw. Symp. Dig.*, Jun. 2008, pp. 1027–1030.
- [17] S.-F. Chao, C.-H. Wu, Z. M. Tsai, H. Wang, and C. Chen, "Electronically switchable bandpass filters using loaded stepped-impedance resonators," *IEEE Trans. Microw. Theory Tech.*, vol. 54, no. 12, pp. 4193–4201, Dec. 2006.
- [18] M. A. El-Tanani and G. Rebeiz, "A two-pole two-zero tunable filter with improved linearity," *IEEE Trans. Microw. Theory Tech.*, vol. 57, no. 4, pp. 830–839, Apr. 2009.

Andrew C. Guyette (M'08) was born in Grand Forks, ND, in 1976. He received the B.S. and M.S. degrees in electrical engineering from the University of Hawaii at Manoa, in 1999 and 2001, respectively, and the Ph.D. degree from The University of Leeds, Leeds, U.K., in 2006.

Since 2007 he has been with the Naval Research Laboratory, Washington, DC. His research interests include tunable filters, lossy filters, and network synthesis.